Catalysis Today 187 (2012) 48–55

Contents lists available at SciVerse ScienceDirect

Catalysis Today

journal homepage: www.elsevier.com/locate/cattod

$Cu_xCr_yO_z$ mixed oxide as a promising support for gold – The effect of Au loading method on the effectiveness in oxidation reactions

Izabela Sobczak[a,*], Katarzyna Szrama[a], Robert Wojcieszak[b], Eric M. Gaigneaux[b], Maria Ziolek[a]

[a] A. Mickiewicz University, Faculty of Chemistry, Grunwaldzka 6, 60-780 Poznań, Poland
[b] Université catholique de Louvain, Institute of Condensed Matter and Nanosciences – IMCN, Molecules, Solids and Reactivity – MOST, Croix du Sud 2/17, B-1348 Louvain-la-Neuve, Belgium

ARTICLE INFO

Article history:
Received 27 June 2011
Received in revised form 7 September 2011
Accepted 30 September 2011
Available online 6 November 2011

Keywords:
$Au/Cu_xCr_yO_z$
CO, glycerol and methanol oxidation
Effect of gold particles

ABSTRACT

$Cu_xCr_yO_z$ containing copper–chromium oxide spinel and CuO was used as a support for gold loaded by different methods: deposition–precipitation using KOH, deposition–precipitation using urea and gold–sol method with tetrakis(hydroxymethyl)phosphonium chloride. The technique of modification with gold determined not only the Au particle size (the smallest if gold–sol method was used) but also the number of oxygen vacancies and copper concentration on the surface. All these parameters were considered in the study of CO, glycerol and methanol oxidation. The size of gold particles is a key feature determining the activity in the oxidation of CO. Glycerol oxidation is also sensitive to this parameter but less than CO oxidation. The oxidation of methanol is not influenced by the presence of gold and it occurs on the $Cu_xCr_yO_z$ support.

1. Introduction

Supported gold catalysts have been recently extensively studied because of their good catalytic performance in several reactions, including the CO and glycerol oxidation, which are of greatest importance [1–7]. It has been discover that the catalytic properties of gold depend sensitively on a particle size. In the reaction of carbon monoxide oxidation, the catalytic activity increases with decreasing size of gold particles [1,2,8,9]. The gold containing catalysts have been found more active when metal gold particles are smaller than 5 nm and the method used for preparation of the gold catalyst significantly influences the size of gold nanoparticles. One of the methods most often used for gold catalyst preparation is the deposition–precipitation technique which allows a control of particle size depending on pH and the precipitation inducing agent (urea, hydroxides) [1,2,10]. At pH of the solution of gold chloride between 6 and 10 it is possible to obtain gold particles smaller than 4 nm [1,2]. The other principal factor which has a decisive influence on the activity of gold catalysts is the nature of the support. The support can participate in the reaction and/or stabilize the active gold species [11], at the same time forming gold particles sufficiently small to be effective.

Oxides and mixed oxides are the main supports for gold [1,2]. Recently, chromium $MIICr_2O_4$ (MII = Co, Cu, Fe, Mg) [12] and $MgAl_2O_4$ spinels [13] have been used as supports for Au nanoparticles. It has been reported [12] that the activity of $MIICr_2O_4$ type catalysts in CO oxidation depends on the type of cation and increases with increasing reducibility of the catalysts. The sequence of increasing activity: Au/CoCr(80) > Au/MnCr(26) > Au/FeCr(1), where values in brackets are conversions of CO at 308 K, follows the sequence of decreasing reducibility: Au/CoCr(373) > AuMn(498) > AuFeCr(683), where values in brackets are T_{max} (in K) in H_2TPR. Moreover, it has been suggested [12] that the higher the reducibility of $Au/MIICr_2O_4$ catalyst, the higher the concentration of the surface oxygen vacancies in the stationary state of the reaction, that can be the canters of oxygen activation [14–17]. However, it could not be established whether in the chromium spinels containing gold these vacancies are formed on the support and oxygen adsorbed on them migrates by spill-over to Au particles, or whether they are formed on the support centres at the periphery of Au particles [17].

The properties of Au nanoparticles supported on $MgAl_2O_4$ spinels and their activity in glycerol oxidation with oxygen was studied in [13]. It was shown that the most active catalysts were those characterized by the smallest particle sizes. On the other hand, the surface composition (mainly Al/Mg ratio) and the area of the spinel play an important role in determining the selectivity of the reaction, whereas the gold particle size influences the selectivity only partially. According to the authors, the Al-rich surface promotes the C–C bond cleavage.

In this work, $Cu_xCr_yO_z$ mixed oxide system prepared by calcination of hydrotalcites, has been used as support for gold. The focus was on the effect of the methods of gold introduction onto $Cu_xCr_yO_z$ mixed oxides on the particle size of gold, reducibility of the

* Corresponding author. Tel.: +48 61 8291305.
E-mail address: sobiza@amu.edu.pl (I. Sobczak).

0920-5861/$ – see front matter © 2011 Elsevier B.V. All rights reserved.
doi:10.1016/j.cattod.2011.09.042

catalysts prepared and the activity in the oxidation reactions (methanol, glycerol and carbon monoxide oxidation).

2. Experimental

2.1. Preparation of the $Cu_xCr_yO_z$ support

The $Cu_xCr_yO_z$ mixed oxide was prepared by the standard coprecipitation method according to [18]. A solution containing $Cu(NO_3)_2$ (Aldrich) and $Cr(NO_3)_3$ (Aldrich) (initial Cu:Cr atomic ratio = 1) in 50 cm^3 of water was added dropwise to 200 cm^3 of water at a constant pH (pH 11–12) controlled by the addition of 1 M NaOH under vigorous stirring at 313 K. The resulting slurry was heated for 0.5 h and then filtered, washed with water and dried at 353 K for 24 h. Next the material obtained was calcined at 873 K for 3 h.

2.2. Modification with gold

The $Au/Cu_xCr_yO_z$ catalysts were obtained by three methods: (i) deposition–precipitation using KOH, (ii) deposition–precipitation using urea [19] and (iii) gold–sol method with tetrakis (hydroxymethyl)phosphonium chloride (THPC) [19]. Hydrogen tetrachloroaurate(III) hydrate (Johnson Matthey, UK–USA) was the precursor of the active gold phase (1 wt.% loading as assumed). The prepared materials were calcined at 623 K for 4 h.

2.2.1. Gold–sol method

First, the metallic sol was prepared. A mixture of H_2O (232 cm^3) with 0.2 M NaOH (7.5 cm^3) was stirred before adding 5 cm^3 of diluted THPC (1.2 cm^3 of the 78 wt.% solution diluted with 100 cm^3 H_2O). After 2 min of stirring, the gold aqueous solution was added (1 wt.% of Au). The gold–sol was then stirred for 1 h. Aqueous suspension of the support (5 g) was agitated for 15 min in an ultrasonic bath. The gold–sol was added into the support suspensions and stirred for 1 h for immobilisation. The suspension was filtered off, washed until the filtrate was free of chloride ($AgNO_3$ test) and dried at 373 K.

2.2.2. Deposition–precipitation with urea

An aqueous solution of $HAuCl_4$ (calculated as 1 wt.% of Au) was added to a stirred 0.84 M aqueous solution of urea (Fluka) and heated to 353 K on stirring. Then, 5 g of the support was added and the suspension was stirred at 353 K for 4 h. The suspension was filtered off, washed until the filtrate was free of chloride ($AgNO_3$ test) and dried at 373 K.

2.2.3. Deposition–precipitation with KOH

A portion of 5 g of the support was added to 500 cm^3 of $HAuCl_4$ solution (calculated as 1 wt.% of Au) at a constant pH 7.0 (controlled by addition of a KOH 0.2 M solution) and at 433 K. The precipitates obtained were mixed at the same temperature for 1 h, then filtered off, washed until the removal of free of chloride ($AgNO_3$ test) and dried at 373 K.

The following notation is used for the catalyst samples prepared: (sol) denotes gold–sol method, (DPU) stands for the deposition–precipitation method with urea, and (DPK) stands for the deposition–precipitation method with KOH.

2.3. Catalysts characterization

The XRD patterns were obtained on a D8 Advance diffractometer (Bruker) using Cu Kα radiation (λ = 0.154 nm), with a step size of 0.05° in the 2Θ = 6–60° range.

The XPS analyses were performed with a SSI-X-probe (SSX-100/206) photoelectron spectrometer equipped with a monochromatic microfocused Al Ka X-ray source (1486.6 eV) from Surface Science Instruments. The powdered samples were pressed into small stainless steel troughs mounted on a multi-specimen holder. The samples were outgased overnight under vacuum (10^{-7} Torr) and then introduced into the analysis chamber where the pressure was at about 10^{-8} Torr. An electron flood gun set at 8 eV and a Ni grid placed at 3 mm above the sample were used to standardize charging effects. Pass energy of the analyser was 150 eV and the spot size was approximately 1.4 mm^2. The atomic concentration ratios were calculated by normalizing surface area ratios with sensitivity factors based on Scofield cross-sections. In addition, all binding energies were calculated taking as a reference the C–(C, H) component of the C 1s adventitious carbon peak fixed at 284.8 eV. Peak decomposition was performed using the CasaXPS program (Casa Software Ltd., UK) with a Gaussian/Lorentzian (85/15) product function and a Shirley nonlinear sigmoid-type baseline. The following peaks were used for the quantitative analysis: O 1s, C 1s, Cu 2p, Cr 2p, Cl 2p, Na 1s and Au 4f. For Au 4f peak, the theoretical distance between Au 4f5/2 and Au 4f7/2 peaks was 3.67 eV and the area ratio was 3/4. For Cr 2p the area ratio and theoretical distance between Cr 2p3/2 and Cr 2p1/2 peaks were taken 2/3 and 10 eV, respectively. For Cu 2p the same area ratio was taken with the theoretical distance of 19.9 eV. Moreover, the LMM Auger peak of Cu at 570 eV was also monitored. Particle size was estimated from the intensity ratio of Au 4f and Cr 2p using slab model introduced by Kerkhof–Moulijn [20]. This model depends strongly on the physical properties of the support. It is based on the metal loading and the specific surface area of the catalysts.

The temperature-programmed reduction (TPR) of the samples was carried out using H_2/Ar (10 vol.%) as a reducing agent (flow rate = 40 cm^3 min^{-1}). The sample (4 mg) was packed in a quartz tube, treated in a flow of helium at 623 K and cooled to room temperature (RT). Then the sample was heated at a rate of 10 K min^{-1} to 1273 K in the presence of the reducing mixture. Hydrogen consumption was measured by a thermal conductivity (TCD) detector.

The 2-propanol conversion (dehydration and dehydrogenation) was performed using a microcatalytic pulse reactor inserted between the sample inlet and the column of a CHROM-5 chromatograph. The catalyst bed (0.05 g) was first activated at 623 K for 2 h under helium flow (40 cm^3 min^{-1}). The 2-propanol (Aldrich) conversion was studied at 423, 473, 523 and 573 K using 3 μl pulses of alcohol under helium flow (40 cm^3 min^{-1}). The reactant and the reaction products: propene, 2-propanone (acetone) and diisopropyl ether were analysed using CHROM-5 gas chromatograph on line with microreactor. The reaction mixture was separated on 2 m column filled with Carbowax 400 (80–100 mesh) at 338 K in helium flow (40 cm^3 min^{-1}) and detected by TCD.

2.4. Oxidation reactions

2.4.1. Glycerol oxidation

The glycerol oxidation experiments were performed in a 300 cm^3 batch reactor from Parr. The oxidation reactions were carried out with oxygen under pressure of 6 atm, at 333 and 353 K. 0.8 g NaOH (NaOH/glycerol molar ratio = 2) and 0.2 g of gold catalyst were added to a 1 M aqueous solution of glycerol. The reaction mixture was stirred (1500 rpm) for 5 h. The quantitative analyses of the reaction mixtures were performed by high performance liquid chromatography (HPLC). The analysis was carried out using a HPLC chromatograph (Waters) equipped with ultraviolet (UV) and refractive index (RI) detectors. The reactant and the products were separated on an ion exclusion column (IC-Pak Ion Exclusion 7.8 × 300 mm – Waters) heated at 343 K. The eluent was a solution of H_2SO_4 (0.0004 M). The samples were taken at the end of the

reactions, 1 cm^3 of the sample was diluted in 10 cm^3 of water and 5 μl of this solution was analysed.

2.4.2. Oxidation of methanol

Oxidation of methanol was performed in a fixed-bed flow reactor. The pressed material was granulated to 0.5 < ∅ < 1 mm size fraction. A portion of 0.1 g of the catalyst, was placed in the reactor. The samples were activated in helium flow (40 cm^3 min^{-1}) at 623 K for 2 h. Next the temperature was decreased to the desired reaction temperature. The gas mixture of MeOH and O_2 (O_2/MeOH molar ratio = 2), diluted by He, was used with a total flow rate of 40 cm^3 min^{-1}. The reactor effluent was analysed using an online gas chromatograph (GC 8000 Top) equipped with FID and TCD detectors. Helium was used as a carrier gas. Products were separated on a 60 m DB-1 column, which was kept at 313 K.

2.4.3. CO oxidation

The CO oxidation was studied in the temperature range 308–473 K using 0.1 g of the catalyst sample (0.5 < ∅ < 1 mm size fraction). The samples were activated in argon flow (40 cm^3 min^{-1}) at 623 K for 2 h. The volume ratio of the components of the reaction mixtures was – $CO:O_2$:Ar = 1:5:44 vol.%. The reactor effluent was analysed using an online gas chromatograph (GC 8000 Top) equipped with a TCD detector.

3. Results and discussion

3.1. The structure and chemical composition of $Cu_xCr_yO_z$ mixed oxides – the effect of modification with gold

The structure of copper–chromium oxides before and after modification with gold was studied by XRD technique. Powder XRD patterns of the calcined catalysts are shown in Fig. 1A and B. The diffractogram of $Cu_xCr_yO_z$ oxide consists of two intense peaks at 2Θ = 35.5° (100% intensity), 38.7° and the lower intensity peaks at 2Θ = 32.5°, 48.7°, 53.5°, 58.4°, all characteristic of well dispersed CuO crystallites [ICDD PDF 065-2309]. Moreover, the XRD pattern exhibits several peaks at 2Θ = 18.6, 29.3, 31.1, 35.1 (100% intensity) 37.7, 42.2, 46.6, 53.4, 56.2, 57, 9) belonging to the phase of $CuCr_2O_4$ [ICDD PDF 00-034-0424] [21]. It indicates that the copper–chromium mixed oxide obtained is a mixture of CuO and the spinel phase of chromite $CuCr_2O_4$, similarly as shown in [22]. The latter one has a structure of rutile as indicated in Fig. 1 by comparison with XRD data [ICDD PDF 00-034-0424]. The XPS data indicate the presence of Cr^{3+} (the Cr $2p_{3/2}$ binding energies at 576.31 eV) and Cu^{2+} (the Cu $2p_{3/2}$ binding energies at 932.04 eV with a shoulder at 933.84 eV) [21,23,24], as dominating cationic species on the support surface. It confirms the formation of a mixed copper–chromium oxide such as $CuCr_2O_4$ as shown by XRD results. The SEM micrograph of $Cu_xCr_yO_z$ material (not shown here) gives information about the morphology of the sample. It shows that the oxide composition is essentially homogeneous, with local compositional inhomogeneities. It is worth noting that the structure and morphology of $Cu_xCr_yO_z$ sample is not affected after introduction of gold, irrespective of the method of modification by gold.

Contrary, the modification with gold gives rise to significant changes in the bulk and surface composition of $Cu_xCr_yO_z$ concluded,

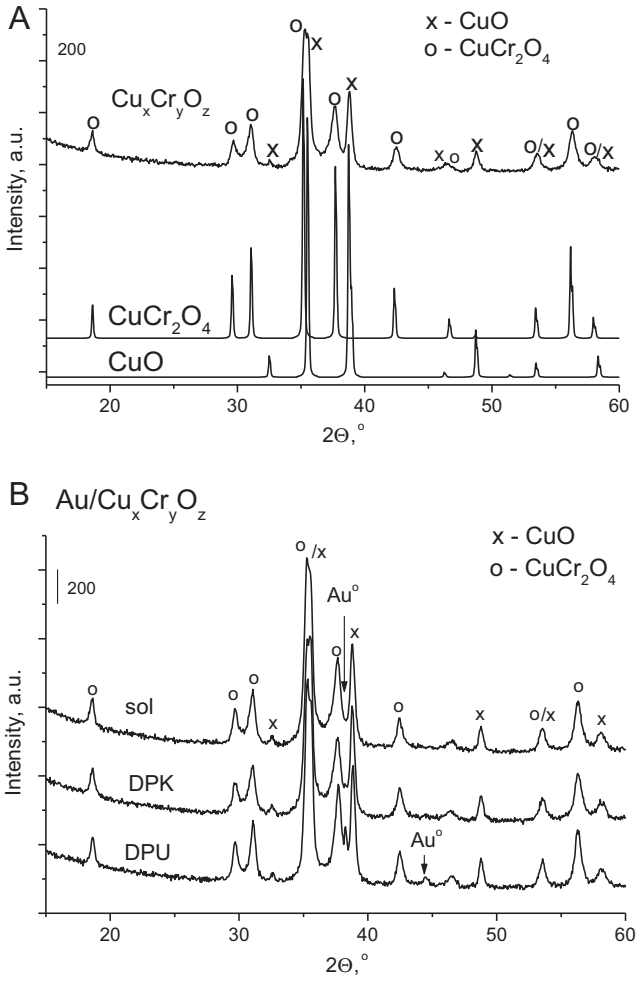

Fig. 1. XRD patterns of $Cu_xCr_yO_z$ matrix, CuO (ICDD PDF 065-2309) and $CuCr_2O_4$ oxide (rutile) (ICDD PDF 00-034-0424) (A); $Au/Cu_xCr_yO_z$ (sol), $Au/Cu_xCr_yO_z$ (DPK), $Au/Cu_xCr_yO_z$ (DPU) (B).

respectively, from ICP and XPS results. The chemical compositions of copper–chromium oxide catalysts before and after the gold introduction by different methods are listed in Tables 1 and 2. The data clearly show that the amount of metals, calculated from XPS and ICP data, in the $Cu_xCr_yO_z$ matrix differs from that in the samples after modification with gold. The ICP results indicate that the modification leads to an increase in the Cu:Cr molar ratio in the sample (from 1.00 to 1.05 depending on the method of Au loading). It is important to note that both, Cr and Cu, are partially removed

Table 2
Gold loading and gold particle size in $Cu_xCr_yO_z$ oxides.

Catalyst	Au, wt.% ICP	Particle size XPS [nm]	Particle size XRD [nm]
$Au/Cu_xCr_yO_z$ (sol)	0.85	2.3	–
$Au/Cu_xCr_yO_z$ (DPU)	0.92	1.2	32
$Au/Cu_xCr_yO_z$ (DPK)	0.64	6.8	–

Table 1
Chemical composition of $Cu_xCr_yO_z$ oxides – ICP and XPS results.

Catalyst	Cu:Cr (mol) ICP	Cu:Cr XPS	Cr, % XPS	Cu, % XPS	O, % XPS
$Cu_xCr_yO_z$	1:1 (1.00)	0.71	17.6	12.5	57.1
$Au/Cu_xCr_yO_z$ (sol)	0.99:0.97 (1.02)	0.90	14.8	13.4	52.6
$Au/Cu_xCr_yO_z$ (DPU)	0.99:0.94 (1.05)	0.81	16.1	13.0	53.4
$Au/Cu_xCr_yO_z$ (DPK)	0.99:0.95 (1.04)	0.76	16.5	12.5	54.9

during Au loading and that removal of chromium is much greater than that of copper. Moreover, the decrease in chromium content is higher for samples modified by the deposition–precipitation than by the sol method. Similarly, the increase in the Cu:Cr molar ratio on the surface of all gold modified samples was observed by XPS method. However, contrary to the bulk, the decrease in chromium content on the surface is the highest for the sample modified by the gold–sol method. The chromium removal from the sample is rather not the effect of stirring time of the support with the solution of chloroauric acid. The time of stirring for DPU is much longer than in the case of DPK (4 and 1 h, respectively), whereas the level of chromium removal is similar. The different interaction between gold species and chromium cations during the modification procedure that determines the removal of chromium can be proposed. In the gold–sol method metallic gold is formed and it can act as reducing agent for Cr^{3+} as Zn/Hg (used usually). Cu^{2+} can form $CrCl_2$ (chloride ions are present in the solution) easily dissolved in water. It causes the leaching of chromium from the solid. Contrary, during deposition–precipitation methods $AuCl(OH)_3^-$ and $Au(OH)_4^-$ ions are present and they interact with the cationic Cr^{3+}. Such interaction can make the migration of Cr^{3+} from the bulk to the surface. It causes the higher content of chromium on the surface of the final material.

The decrease in chromium content on the surface of $Au/Cu_xCr_yO_z$ is accompanied by the decrease in the content of surface oxygen species and an increase in the copper content. A possible explanation is the migration of copper cations from the bulk to the surface position former occupied by released chromium cations. The decrease in surface oxygen (XPS results – Table 1) indicates the formation of vacancies. This phenomenon can be explained by weakening of metal–oxygen bonds in $Cu_xCr_yO_z$ upon interaction with gold loaded as postulated by Nolan et al. [25,26] for Au modified ceria.

Table 2 presents the data on the gold loading in mixed oxides. The data clearly show that the amount of gold in the final gold-containing materials differs depending on the method of modification. The metal loading in all samples is lower than assumed (<1 wt.%). The gold loading is higher in $Au/Cu_xCr_yO_z$ (DPU) and $Au/Cu_xCr_yO_z$ (sol) than in $Au/Cu_xCr_yO_z$ (DPK) sample.

3.2. The state of gold and the size of gold crystallites

The state of gold in the $Cu_xCr_yO_z$ catalysts prepared was studied by XPS and XRD techniques. XPS results indicate that metallic gold is present on the surface of all gold-modified samples (in the XPS spectra of Au 4f region there is a peak centred at 83.95 eV which is typical of supported gold [27] and similar to the energies of metallic Au described in the literature [23]). It is important to note, that the low intensity of the Au 4f peaks in the 83–86 eV range (at the limit of detection), did not permit to deduce the presence (or absence) of cationic gold.

XRD patterns (Fig. 1B) confirm the presence of metallic gold on the surface of $Au/Cu_xCr_yO_z$ catalysts. The reflections characteristics of metallic gold (at $2\Theta = 38.2^\circ$ and 44.4°) [28,29] are well visible for the catalyst prepared by DPU method. Only very low intense XRD reflection from metallic gold at $2\Theta = 38.2^\circ$ is present for the $Au/Cu_xCr_yO_z$ (DPK) catalyst. In contrast, in the XRD patterns of $Au/Cu_xCr_yO_z$ modified by gold–sol method the peaks corresponding to metallic gold were not detected. The results clearly indicate that the size of metallic gold crystallites is determined by the method of Au introduction. The size of the gold nanoparticles was estimated by XRD using the Scherrer formula [30] and XPS intensity ratios using models proposed by Kerkhof and Moulijn [20]. The results are shown in Table 2. Much greater Au agglomerates are formed on Au/oxide prepared by the deposition–precipitation methods with KOH (average particle size

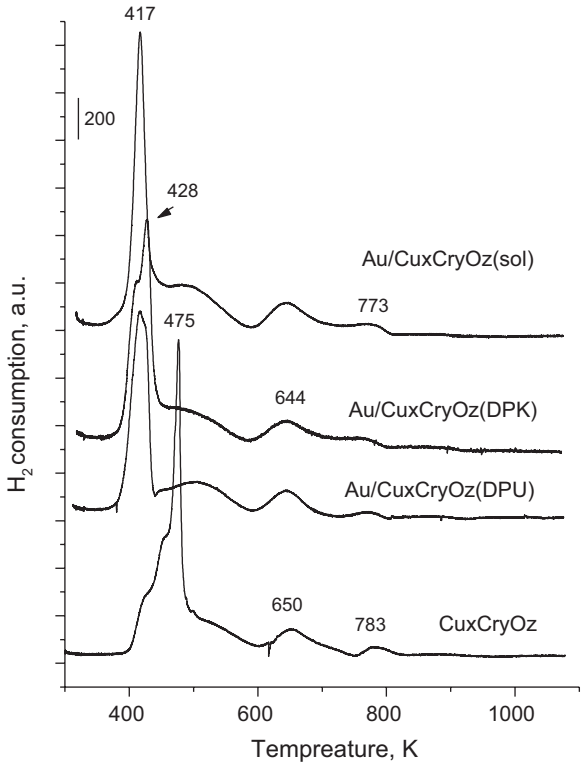

Fig. 2. H_2-TPR curves for $Au/Cu_xCr_yO_z$ catalysts and the support.

calculated from XPS ~ 7 nm) than when the gold–sol method with the use of THPC as a reducing and stabilizing agent is applied (average particle size ~2 nm). THPC stabilizes the colloid gold solutions and that is why gold particles size is smaller and their dispersion is greater. This finding is consistent with XRD studies showing the peak from metallic gold crystallites only for the sample with crystallites greater than 5 nm ($Au/Cu_xCr_yO_z$ (DPK)). On the other hand, it is known that XPS analysis is very sensitive to the very small particles. It has been proved in [31] that the XRD data provide information on the size of the largest particles only, while the XPS on the size of the smallest present particles. It is the reason for different results from XRD and XPS studies obtained for $Au/Cu_xCr_yO_z$ (DPU) sample. The average particle size estimated from XRD diffraction pattern for this sample is about 32 nm, whereas from XPS intensity ratios it is of about 1 nm. It indicates that on the surface of the catalysts prepared by DP method with urea, the fraction of greater (~32 nm) and smaller particles (~1 nm) coexists.

3.3. Reducibility of the catalysts – H_2-TPR

The H_2-TPR profiles of $Cu_xCr_yO_z$ and $Au/Cu_xCr_yO_z$ catalysts are shown in Fig. 2. They show two distinct regions in the temperature range of 400–550 K and 600–800 K. Two peaks in the TPR profile of $Cu_xCr_yO_z$, a strong one at 475 K and a shoulder at 500 K, originate from the reduction of CuO crystallites dispersed over the support [32–34]. The first is due to the reduction of the highly dispersed CuO, whereas the second to the reduction larger CuO aggregates [35]. The other broad peaks at 650 and 783 K are due to the reduction of $Cu_xCr_yO_z$ species [21,33]. These results are in agreement with the chemical phase composition estimated from XRD and XPS studies.

H_2-TPR measurements show a marked effect of Au particles on the reducibility of $Cu_xCr_yO_z$ support, similarly as shown in [12] for MCr_2O_4 (M = Cu, Co, Mn, Mg) oxides. Fig. 2 indicates that the deposition of Au nanoparticles, irrespective of the method of gold

Table 3
The results of 2-propanol decomposition at various temperatures.

Catalyst	React. temp. (K)	Conversion i-PrOH (%)	Selectivity (%) towards	
			Propene	Acetone
$Cu_xCr_yO_z$	423	3	Traces	100
	473	46	Traces	100
	573	100	5	95
$Au/Cu_xCr_yO_z$ (sol)	423	38	Traces	100
	473	88	Traces	100
	573	97	3	97
$Au/Cu_xCr_yO_z$ (DPU)	423	24	1	99
	473	93	2	98
	573	99	3	97
$Au/Cu_xCr_yO_z$ (DPK)	423	20	1	99
	473	92	1	99
	573	100	3	97

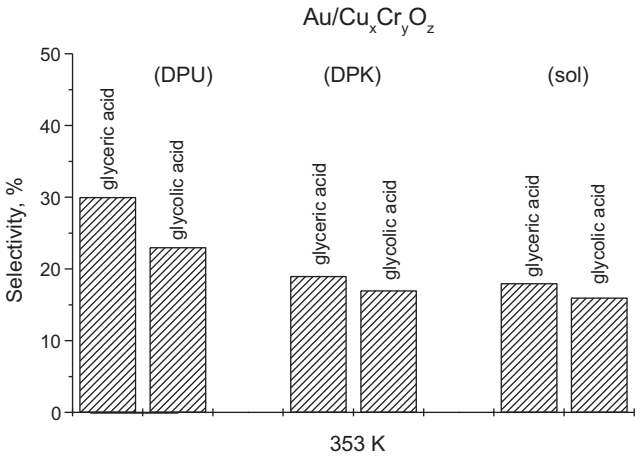

Fig. 3. The selectivity to glyceric and glycolic acids in glycerol oxidation on $Au/Cu_xCr_yO_z$ catalysts.

introduction, leads to the significant decrease in the T_{max}, for both the peak from CuO reduction (from 475 to 417 K) and the peaks assigned to spinel reduction (from 650 to 644 K and 783 to 773 K) in all the samples. The higher effect of Au loading on T_{max} (CuO) than T_{max} (spinel) suggests the location of gold species close to the CuO phase.

It has been reported in the literature [12], that the presence of Au particles facilitates activation (dissociation) of a hydrogen molecule used in H_2-TPR. The dissociated hydrogen species migrate by a spill-over process from the surface of Au particles to the support. Therefore, the influence of gold species on reducibility of the support depends on the gold particle size and concentration of Au species (Table 2). As concerns CuO reduction the most significant effect is observed on $Au/Cu_xCr_yO_z$ (sol).

3.4. Acidity/basicity of the catalysts – 2-propanol decomposition test reaction

The 2-propanol decomposition is a test reaction for characterization of acidic (Brønsted or Lewis) and/or basic properties of solids [36]. Dehydration of alcohol to propene and/or di-isopropyl ether requires acidic centres (Lewis or BrØnsted), whereas the dehydrogenation to acetone occurs on the basic sites. It is noteworthy that ether production requires the presence of pairs of Lewis acid–base centres. Some authors (e.g. [37]) have reported that acetone formation takes place on redox centres.

This test reaction allows the estimation of basicity and redox properties of the catalysts applied in this work. As shown in Table 3, over $Cu_xCr_yO_z$ support and all Au containing oxides the main reaction product of 2-propanol decomposition at 423, 473 and 573 K is acetone indicating dehydrogenating properties (basicity or redox properties) of the catalysts. Basic (Lewis) centres originate from the oxygen in CuO and $CuCr_2O_4$, whereas copper and chromium ions are responsible for redox activity. Additionally, at a higher reaction temperature (573 K) a small amount of propene is formed, indicating slight activity of the acidic centres. It is evident that gold introduction generates new active centres and significantly increases the activity of $Cu_xCr_yO_z$ oxides towards alcohol decomposition, that is especially pronounced at 423 K. Metallic gold nanoparticles are known from their high oxidation power at low temperature and therefore one can conclude that redox properties of catalysts used play an important role in dehydrogenation of 2-propanol to acetone. It is worth of notice that the activity differs depending on the method of gold modification at this temperature and it is the highest on $Au/Cu_xCr_yO_z$ (sol).

3.5. Activity in oxidation reactions – effect of gold particle size

The activity of the catalysts prepared was investigated in CO, glycerol and methanol oxidation with oxygen and the results are given in Table 4. As known from literature, glycerol oxidation is a structure-sensitive reaction [19,38]. The results obtained for $Au/Cu_xCr_yO_z$ catalysts confirmed this statement. Similarly as shown earlier for gold modified carbons [19,38,39], group five metal oxides [10] and $MgAl_2O_4$ spinels [13], the activity of gold catalysts studied in this work in glycerol oxidation depended on the method of gold introduction which determines the Au particle sizes. $Au/Cu_xCr_yO_z$ prepared by the gold–sol method, which leads to the lowest gold particle sizes, show a higher activity than the catalyst prepared by the deposition–precipitation (Table 4). The increase in the reaction temperature from 333 K to 353 K causes a significant increase in the glycerol conversion for all the catalysts.

As far as the selectivity in glycerol oxidation over $Au/Cu_xCr_yO_z$ catalysts is concerned, it was the highest to glyceric and glycolic acids. Other products of oxidation formed include: tartronic, oxalic and formic acids. However, the yields of these products are low. It is important to stress the influence of gold particle sizes on the selectivity towards the products of glycerol oxidation (glyceric and glycolic acids). For $Au/Cu_xCr_yO_z$ (DPU) catalyst with the domination of large gold particles (gold particles about 30 nm) the selectivity to glyceric acid was significantly higher than to glycolic acid (Fig. 3). Moreover, the selectivity to glyceric acid over this catalyst is the highest (30% at 353 K) from among all catalysts studied. For the catalysts with smaller gold particles (in the range 2–7 nm) the selectivity to both acids at 353 K (it means at temperature of a higher conversion) is similar, indicating the higher transformation of glyceric to glycolic acid on small gold particles. It is worth noting that the influence of metal particle size on the selectivity of $Au/Cu_xCr_yO_z$ catalysts is not as clearly evidenced as for gold modified carbons [19,38], for which the small gold particles play an important role in the oxidation of glyceric to glycolic acid. It was found [19] that on Au/C catalysts with small gold particle size (<3 nm) the selectivity to glyceric acid significantly decreased and much higher selectivity to glycolic acid was obtained in comparison to catalysts with gold particle size in the range 3–45 nm. It is important to stress, that the increase in the reaction temperature from 333 K to 353 K causes a significant change in the products selectivity. For the most active $Au/Cu_xCr_yO_z$ (sol) catalysts the decrease of the selectivity to glyceric and tartronic acids is observed, whereas the selectivities to glycolic and formic acids are enhanced at higher temperature

Table 4
Catalytic activity in glycerol + O_2, MeOH + O_2 and CO + O_2 oxidation reactions.

Catalyst	CO oxidation		Glycerol oxidation				MeOH oxidation				
	Temp. (K)	Conv. (%)	Temp. (K)	Conv. (%)	Sel. to glyceric acid (%)	Sel. to glycolic acid (%)	Temp. (K)	Conv. (%)	Select. HCHO (%)	Select. $HCOOCH_3$ (%)	Select. CO_2 (%)
$Cu_xCr_yO_z$	323	0	333	15	10	14	473	94	1	–	99
$Au/Cu_xCr_yO_z$ (sol)	308	43	333	29	21	12	423	17	0	19	81
	323	50	353	46	18	16	473	99	0	1	99
$Au/Cu_xCr_yO_z$ (DPU)	308	9	333	21	18	14	423	12	0	29	71
	323	11	353	32	30	23	473	100	0	0	100
$Au/Cu_xCr_yO_z$ (DPK)	308	6	333	26	22	20	423	16	0	39	61
	323	9	353	41	19	17	473	99	0	0	100

(Fig. 4). It indicates that temperature promotes the oxidation of glyceric acid to other products of oxidation.

The oxidation of glycerol to glyceric acid most probably proceeds via initial formation of glyceraldehyde, which is rapidly oxidized to glyceric acid [19]. Further oxidation of glyceric acid leads to tartronic acid which would be expected to undergo facile decarboxylation to give glycolic acid [7] (Scheme 1). The glycerol oxidation is a typical consecutive reaction proceeding according to the rake model [10]. In such a process the selectivity is strongly determined by the adsorption and desorption rate of each product. Thus, the relation between the rate of desorption of glyceric acid and the rate of its oxidation to tartronic acid determines the selectivity to one or the other product. The faster the desorption of glyceric acid (from the larger Au particles) the lower the selectivity to tartronic and glycolic acids.

The fact that the role of Au particle size in glycerol oxidation on $Au/Cu_xCr_yO_z$ is not so significant as on Au/C catalysts suggests that the pristine support is also active in this reaction as documented by the results in Table 4.

The effect of gold particle size on the activity of $Au/Cu_xCr_yO_z$ catalysts is much more pronounced in CO oxidation reaction (Table 4). Fig. 5 shows the CO conversion as a function of temperature over $Au/Cu_xCr_yO_z$ catalysts prepared by different methods. The sample prepared by the gold–sol method (average gold particle size ca. 2 nm) showed a much higher CO oxidation activity at low temperature (308 K) than the catalysts prepared by the deposition–precipitation methods. The activity increased with the reaction temperature. This observation is in agreement with the literature data indicating that small gold particles are more active than large ones in the oxidation of carbon monoxide, with a maximum activity found for the particles with an average diameter ca. 3 nm [1,8,9]. The activity of $Au/Cu_xCr_yO_z$ (DPU) and $Au/Cu_xCr_yO_z$ (DPK) samples in CO oxidation is similar. Both samples contain much higher gold particles and it is a reason of their much lower activity in CO oxidation in comparison with $Au/Cu_xCr_yO_z$ (sol). $Au/Cu_xCr_yO_z$ (DPU) has two fractions of crystallites, very big (ca. 32 nm) and small (ca. 1 nm), whereas the mean particle size for $Au/Cu_xCr_yO_z$ (DPK) is ca. 6 nm (Table 2). Another important factor is reducibility of the catalyst, which significantly increases after gold modification. The higher the reducibility, the higher the concentration of the surface oxygen vacancies as the centres of the oxygen activation and in a consequence a higher catalyst activity in CO oxidation [12]. However, the reducibility of the support is not a key factor because of similar reducibilities of $Au/Cu_xCr_yO_z$ (DPU) and $Au/Cu_xCr_yO_z$ (sol) do not lead to the same activity in CO oxidation. It indicates that particle size is more important than the effect of

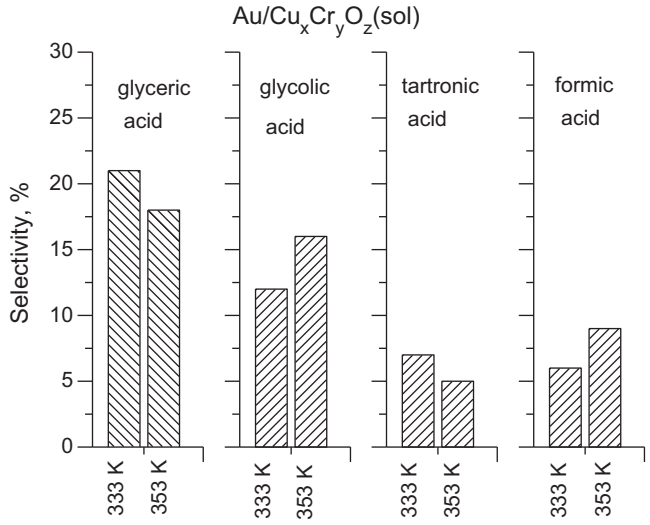

Fig. 4. The selectivity to glyceric, glycolic, tartronic and formic acids in glycerol oxidation on $Au/Cu_xCr_yO_z$ (sol) catalyst – effect of the reaction temperature.

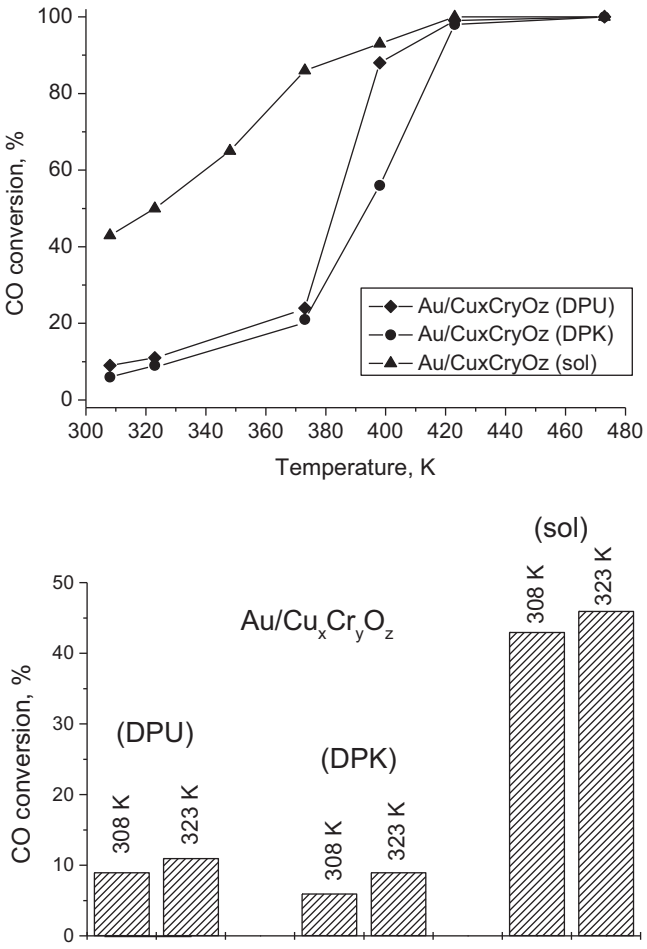

Fig. 5. CO conversion on $Au/Cu_xCr_yO_z$ catalysts – effect of the reaction temperature.

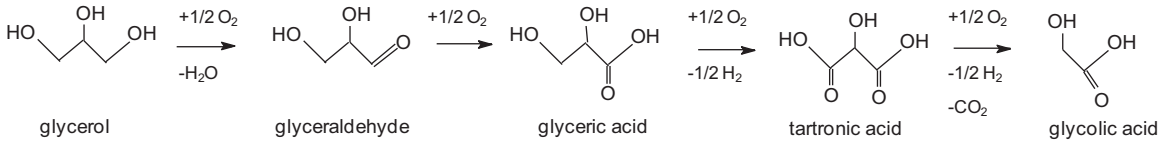

Scheme 1. Possible reaction pathway for glycerol oxidation.

support reducibility for high activity. However, it cannot be excluded that both parameters are important as shown for $Au/Cu_xCr_yO_z$ (sol) sample. Taking it into consideration, the mechanism typical of reducible oxides [1] can be proposed for CO oxidation on $Au/Cu_xCr_yO_z$ catalysts. This mechanism involves the role of gold particles and the support with the oxide ion vacancies on the surface [1]. Such vacancies can be generated as a result of gold–support interaction (Section 3.1) or they are a result of thermal desorption or reduction with carbon monoxide spilling over from the metal (CO adsorbed on metal surface spills onto the support and removes oxygen from the lattice leaving anion vacancies at the surface [40]). Oxygen molecules may adsorb at these vacancies as O_2^- and then migrate by spill-over to gold particles. The distance of migration is less as the particle size decreases and that is why the number of activated oxygen species close to the gold particles increases [41]. The O_2^- superoxide ion can dissociate at the particle edge before reacting with carbon monoxide [16].

The oxidation of methanol is a more complicated process. Methanol oxidation involves the formation of chemisorbed methoxy groups on acidic sites [42–44] with participation of nucleophilic oxygen (basic sites) or redox centres [44,45]. Methoxy species are further transformed to formaldehyde (FA) resulting from the extraction of hydrogen [42,43]. If FA is chemisorbed strongly enough on nucleophilic sites it can interact with the next MeOH molecule and form methyl formate (MF). The chemisorption of MeOH on pairs of active centres is also possible and leads to formate species which further interact with MeOH towards MF. The total oxidation of MeOH to CO_2, usually involving the radical mechanism, points to the basic character of the catalyst. The results of MeOH oxidation at 423 and 473 K on all $Au/Cu_xCr_yO_z$ catalysts studied in this work are shown in Table 4. It is clear that gold catalysts based on $Cu_xCr_yO_z$ mixed oxide are highly active in MeOH conversion to CO_2 at 473 K but the pristine support is also highly active in this reaction. The oxidation of methanol to CO_2 can proceed in the radical reaction on basic centres or step by step with the oxidation to formaldehyde and formic acid on redox centres. The basicity originates from nucleophilic oxygen on the support surfaces (oxygen bonded to copper in CuO and $CuCr_2O_4$ phases) or it can be O_2 chemisorbed on the defect holes. It is important to note that at lower temperature (423 K) and lower MeOH conversion, methyl formate is formed besides CO_2. It suggests the participation of the mechanism of total MeOH oxidation proposed in [42] via formation of formaldehyde (strongly adsorbed on the active centres) and next formic acid oxidized to CO_2.

The results obtained indicate that the presence of gold and gold particle size do not play any role in the oxidation of methanol on $Au/Cu_xCr_yO_z$ catalysts.

4. Conclusions

$Cu_xCr_yO_z$ mixed oxides prepared within this study contain both spinel copper–chromium oxide and CuO phases. The gold loading creates oxygen vacancies, causes partial removal of chromium cations and migration of copper from the bulk to the surface. All these effects are determined by the method applied for the modification with gold. The use of gold–sol technique leads to the highest oxygen deficit and copper concentration on the surface. It also causes generation of the smallest metallic gold particles.

The size of gold particles is a key feature determining the activity in the oxidation of CO. Glycerol oxidation is also sensitive to this parameter but to a lesser degree than CO oxidation. The oxidation of methanol is not influenced by the presence of gold and it occurs on the $Cu_xCr_yO_z$ support. The slight increase in methanol conversion after gold loading can be correlated with the increase in reducibility of the support resulting from the presence of gold species.

Acknowledgements

COST action D36, WG No. D36/0006/06 and the Polish Ministry of Science (Grant No. N N204 032536) are acknowledged for the financial support of this work. Acknowledge is made also to Johnson Matthey (UK–USA) for supplying $HAuCl_4$.

References

[1] G.C. Bond, C. Luis, D.T. Thompson, Catalysis by Gold, Imperial College Press, 2006.
[2] G.C. Bond, D.T. Thompson, Catal. Rev. – Sci. Eng. 41 (1999) 319–388.
[3] G.C. Bond, Catal. Today 72 (2002) 5–9.
[4] D.T. Thompson, Appl. Catal. A 243 (2003) 201–205.
[5] G.J. Hutchings, Catal. Today 72 (2002) 11–17.
[6] G.J. Hutchings, M. Haruta, Appl. Catal. A: Gen. 291 (2005) 2–5.
[7] N. Dimitratos, J.A. Lopez-Sanchez, J.M. Anthonykutty, G. Brett, A.F. Carley, R.C. Tiruvalam, A.A. Herzing, Ch.J. Kiely, D.W. Knight, G.J. Hutchings, Phys. Chem. Chem. Phys. 11 (2009) 4952–4961.
[8] G.R. Bamwenda, S. Tsubota, T. Nakamura, M. Haruta, Catal. Lett. 44 (1997) 83–87.
[9] Z. Yan, S. Chinta, A.A. Mohamed, J.P. Fackler Jr., D.W. Goodman, Catal. Lett. 111 (2006) 15–18.
[10] I. Sobczak, K. Jagodzinska, M. Ziolek, Catal. Today 158 (2010) 121–129.
[11] M. Haruta, S. Tsubota, T. Kobayashi, H. Kageyama, M.J. Genet, B. Delmon, J. Catal. 144 (1993) 175–192.
[12] M. Ruszel, B. Grzybowska, K. Samson, I. Gressel, A. Klisinska, Catal. Today 112 (2006) 126–129.
[13] A. Villa, A. Gaiassi, I. Rossetti, C.L. Bianchi, K. van Benthem, G.M. Veith, L. Prati, J. Catal. 275 (2010) 108–116.
[14] H. Liu, A.I. Kozlov, A.P. Kozlova, T. Shida, Y. Iwasawa, Phys. Chem. Chem. Phys. 1 (1999) 2851–2860.
[15] D. Horvath, L. Toth, L. Guczi, Catal. Lett. 67 (2000) 117–128.
[16] M.M. Schubert, S. Hackenberg, A.C. van Veen, M. Muhler, V. Plzak, R.J. Behm, J. Catal. 197 (2001) 113–122.
[17] B. Grzybowska-Swierkosz, Catal. Today 112 (2006) 3–7.
[18] V.R. Choudhary, D.K. Dumbre, B.S. Uphade, V.S. Nerkhede, J. Mol. Catal. A: Chem. 215 (2004) 129–135.
[19] S. Demirel-Gulen, M. Lucas, P. Claus, Catal. Today 102–103 (2005) 166–172.
[20] F.P.J.M. Kerkhof, J.A. Moulijn, J. Phys. Chem. 83 (1979) 1612–1619.
[21] G. Pantaleo, L.F. Liotta, A.M. Venezia, G. Deganello, E.M. Ezzo, M.A. El Kherbawi, H. Atia, Mater. Chem. Phys. 114 (2009) 604–611.
[22] K. Bahranowski, E. Bielańska, J. Janas, T. Machej, L. Matachowski, E.M. Serwicka, J. Polish, Environ. Stud. 6 (1997) 59–63.
[23] J.F. Moulder, W.F. Stickle, P.E. Sobol, K.D. Bomben, Handbook of X-ray Photoelectron Spectroscopy, Perkin–Elmer Corporation, Physical Electronics Division, Eden Prairie, 1992.
[24] F.M. Capece, V. Dicastro, C. Furlani, G. Mattogno, C. Fragale, M. Gargano, M. Rossi, J. Electron. Spectrosc. Relat. Phenom. 27 (1982) 119–128.
[25] M. Nolan, V. Soto, H. Metiu, Surf. Sci. 602 (2008) 2734–2742.
[26] M. Nolan, J. Chem. Phys. 130 (2009) 1447021–1447029.
[27] J. Radnik, C. Mohr, P. Claus, Phys. Chem. Chem. Phys. 5 (2002) 172–177.
[28] C. Kan, W. Cai, Z. Li, G. Fu, L. Zhang, Chem. Phys. Lett. 382 (2003) 318–324.
[29] A.C. Gluhoi, X. Tang, P. Marginean, B.E. Nieuwenhuys, Topics Catal. 39 (2006) 101–110.
[30] G. Bergeret, P. Gallezot, in: G. Ertl, H. Knozinger, J. Weitkamp (Eds.), Handbook of Heterogeneous Catalysis, vol. 2, VCH, Weinheim, 1997, pp. 439–464.
[31] R. Wojcieszak, M.J. Genet, P. Eloy, P. Ruiz, E.M. Gaigneaux, J. Phys. Chem. C 114 (2010) 16677–16684.

[32] S. Kameoka, M. Okada, A.P. Tsai, Catal. Lett. 120 (2008) 252–256.
[33] C.C. Chien, W.P. Chuang, T.J. Huang, Appl. Catal. A: Gen. 131 (1995) 73–87.
[34] J. Xiaoyuan, L. Liping, C. Yingxu, Z. Xiaoming, J. Mol. Catal. A: Chem. 197 (2003) 193–205.
[35] F.-W. Chang, W. Yao, L.K. Chan, Appl. Catal. A: Gen. 246 (2003) 253–264.
[36] A. Gervasisni, J. Fenyvesi, A. Auroux, Catal. Lett. 43 (1997) 219–228.
[37] C. Lahousse, J. Bachelier, J.C. Lavalley, H. Lauron-Pernot, A.M. Le Govic, J. Mol. Catal. 87 (1994) 329–332.
[38] W.C. Ketchie, Y.-L. Fang, M.S. Wong, M. Murayama, R.J. Davis, J. Catal. 250 (2007) 94–101.
[39] S. Demirel, P. Kern, M. Lucas, P. Claus, Catal. Today 122 (2007) 292–300.
[40] R. Green, P. Morrall, M. Bowker, Catal. Lett. 98 (2004) 129–133.
[41] J.D. Grunwaldt, A. Baiker, J. Phys. Chem. B 103 (1999) 1002–1112.
[42] J.M. Tatibouet, Appl. Catal. A: Gen. 148 (1997) 213–252.
[43] G. Busca, A.S. Elmi, P. Forzatti, J. Phys. Chem. 91 (1987) 5263–5269.
[44] X. Gao, I.E. Wachs, M.S. Wong, J.Y. Ying, J. Catal. 203 (2001) 18–24.
[45] K. Routray, W.Ch. Zhou, J. Kiely, I.E. Wachs, ACS Catal. 1 (2011) 54–66.